Title

Simulating galactic cosmic ray effects: Synergy modeling of murine tumor prevalence after exposure to two one-ion beams in rapid sequence

Authors

Huang, Edward Greg
Wang, Ren-Yi
Xie, Liyang
et al.

Publication Date

2020-05-01

DOI

10.1016/j.lssr.2020.01.001

Peer reviewed

Life Sciences in Space Research 25 (2020) 107–118

Contents lists available at ScienceDirect

Life Sciences in Space Research

journal homepage: www.elsevier.com/locate/lssr

Simulating galactic cosmic ray effects: Synergy modeling of murine tumor prevalence after exposure to two one-ion beams in rapid sequence

Edward Greg Huang[a], Ren-Yi Wang[a], Liyang Xie[a], Polly Chang[c], Gracie Yao[d], Borong Zhang[a], Dae Woong Ham[d], Yimin Lin[a], Eleanor A. Blakely[b], Rainer K. Sachs[a,*]

[a] Department of Mathematics, University of California at Berkeley, United States
[b] Lawrence Berkeley National Laboratory, United States
[c] SRI International, Menlo Park, CA 94025, United States
[d] Department of Statistics, University of California at Berkeley, United States

ARTICLE INFO

Keywords:
Adjustable parameter correlations
High atomic number Z and high energy (HZE) radiations
Non-targeted-effects
95% confidence intervals
Synergy, or antagonism, or incremental effect additivity
NSRL – NASA Space Radiation Laboratory

ABSTRACT

Health risks from galactic cosmic rays (GCR) in space travel above low earth orbit remain a concern. For many years accelerator experiments investigating space radiation induced prevalence of murine Harderian gland (HG) tumorigenesis have been performed to help estimate GCR risks. Most studies used acute, relatively low fluence, exposures. Results on a broad spectrum of individual ions and linear energy transfers (LETs) have become available. However, in space, the crew are exposed simultaneously to many different GCR. Recent upgrades at the Brookhaven NASA Space Radiation Laboratory (NSRL) now allow mixtures in the form of different one-ion beams delivered in rapid sequence. This paper uses the results of three two-ion mixture experiments to illustrate conceptual, mathematical, computational, and statistical aspects of synergy analyses and also acts as an interim report on the mixture experiments' results. The results were interpreted using the following: (a) accumulated data from HG one-ion accelerator experiments; (b) incremental effect additivity synergy theory rather than simple effect additivity synergy theory; (c) parsimonious models for one-ion dose-effect relations; and (d), computer-implemented numerical methods encapsulated in freely available open source customized software. The main conclusions are the following. As yet, the murine HG tumorigenesis experimental studies show synergy in only one case out of three. Moreover, some theoretical arguments suggest GCR-simulating mixed beams are not likely to be synergistic. However, more studies relevant to possible synergy are needed by various groups that are studying various endpoints. Especially important is the possibility of synergy among high-LET radiations, since individual high-LET ions have large relative biological effectiveness for many endpoints.

Selected terminology, symbols, and abbreviations. DER – dose-effect relation; $E(d)$ – DER of a one-ion beam, where d is dose; HG prevalence p – in this paper, p is the number of mice with at least one Harderian gland tumor divided by the number of mice that are at risk of developing Harderian gland tumors (so that in this paper prevalence p can never, conceptually speaking, be greater than 1); IEA – incremental effect additivity synergy theory; synergy level – a specification, exemplified in Fig. 5, of how clear-cut an observed synergy is; mixmix principle – a consistency condition on a synergy theory which insures that the synergy theory treats mixtures of agent mixtures in a mathematically self-consistent way; NTE – non-targeted effect(s); NSNA – neither synergy nor antagonism; SEA – simple effect additivity synergy theory; TE – targeted effect(s); β^* – ion speed relative to the speed of light, with $0 < \beta^* < 1$; SLI – swift light ion(s).

1. Introduction

1.1. One-ion beams

Murine Harderian gland (HG) tumorigenesis induced by exposure to ions in the galactic cosmic ray (GCR) spectrum has long been a NASA concern (Fry et al., 1985; Curtis et al., 1992; Alpen et al., 1993, 1994; Chang et al., 2016; Norbury et al., 2016; Huang et al., 2019). Results on a broad spectrum of ions and linear energy transfers (LETs) have become available through experiments using particle accelerators – either the now-decommissioned Bevalac at the Lawrence Berkeley National Laboratory in Berkeley, California, (see, e.g., Alpen et al., 1993) or, in a

* Corresponding author.
E-mail address: sachs@math.berkeley.edu (R.K. Sachs).

https://doi.org/10.1016/j.lssr.2020.01.001
Received 30 October 2019; Received in revised form 24 December 2019; Accepted 2 January 2020

still-ongoing experiment series (Chang et al., 2016), at the accelerator in Upton, New York utilized by the NASA Space Radiation Laboratory (NSRL).

Until recently, acute-irradiation experiments at such accelerators utilized beams that were nominally one-ion monoenergetic. In the cases of main interest in this paper, shielding in the beam line was avoided as much as possible. The auxiliary file WebSup1 has an additional comment on shielding in its subsection W1.1.1.

1.2. Mixtures of one-ion beams

However, in space the crew are exposed simultaneously to many different GCR (Norbury et al., 2019). It was argued that this discrepancy should be addressed (e.g. Kim et al., 2015; Slaba et al., 2016). Recent upgrades at NSRL now allow mixtures – different ions in the GCR spectrum delivered in rapid sequence. The first HG tumorigenesis mixture experiments were recently completed. Tumor harvest was 16 months after the February 2018 exposures. Each of three mixed field experiments used rapidly sequential acute exposures, without shielding intentionally added, to get a two-ion mixture. The ions, which were used pairwise, are shown in Table 1.

Table 1
Ions used in the three mixtures.

Ion	Z	*SKE*	L	β^*
		MeV/u	**keV/μm**	
^{1}H	1	250	0.4	0.614
^{28}Si	14	260	70	0.623
^{56}Fe	26	600	193	0.793

LET values L are approximate and *SKE* values refer to upstream beam entry. Abbreviations and symbols used here are the following. LET – linear energy transfer; *SKE* – specific kinetic energy; u – baryon number (i.e. neutron number plus proton number); Z – charge number; β^* – ion speed relative to the speed of light.

The experiments whose data is used in the present paper consist of these three mixture experiments, plus most of the HG tumorigenesis experiments performed at the Bevalac, plus one-ion experiments analyzed in Chang et al. (2016), plus later one-ion experiments completed by our group. These data will be called the BEVALAC-NSRL data set. As will be explained in Section 2, the reader has automatic full, free access to this curated data set, and to the open source customized computer program suite used for the calculations in the present paper. At present the BEVALAC-NSRL data set includes 52 one-ion HG experiments using 10 different ions in addition to the three two-component mixtures that are the focus of this paper.

Dose d in cGy will often be the independent variable, fluence – i.e. the total number of particle tracks per unit area of the plane perpendicular to a linear accelerator beam – rarely, equivalent dose in Sv never, and HG prevalence sometimes in an effect-dose relation with dose as the dependent variable. Dose-effect relations (DERs) play a central role in our synergy modeling. Every one-ion DER $E(d)$ considered in the present paper obeys $E(0) = 0$, i.e. E by definition refers only to radiogenic effects, with background effects in unirradiated mice subtracted out. Throughout this paper primes denote derived functions; for example, if $E(d) = d^3$ then $E' = E'(d) = \mathrm{d}[E(d)]/\mathrm{d}d = 3d^2$ and $E'' = 6d$.

1.3. Non-targeted effects (NTE)

1.3.1. Preliminary comments

Henceforth, unless explicitly stated to the contrary, it will be assumed that every DER $E(d)$ obeys the following two conditions. (a) $E(d)$ is twice continuously differentiable on the half-open dose interval $[0, \infty)$; and (b) The slope $E'(d)$ is > 0 on $[0, \infty)$. WebSup1 subsection W1.2 gives comments on the motivations for these requirements.

1.3.2. NTE

Classical radiobiological action produces targeted effects (TE). A direct hit or near miss by any combination of track cores and delta ray (s) produces damage. All one-ion DERs used to model the BEVALAC-NSRL data assume that at large fluence TE action dominates (reviewed, e.g., in Huang et al., 2019). Some assume that at very low fluence NTE – wherein cells directly hit by an ion influence nearby cells through intercellular signaling (Hatzi et al., 2015) – dominate, and are called NTE-also DERs. Others assume NTE are negligible at all doses and are called TE-only DERs. Relevant NTE-also one-ion DERs are very curvilinear, not linear no-threshold (LNT), at very low doses. WebSup1 subsection W1.3 summarizes some relevant literature on NTE modeling in recent radiobiology.

More specifically, experimental and theoretical arguments suggest NTE-also DERs have a high slope $E'(d)$ and a negative second derivative $E''(d)$ at very low doses (Brenner et al., 2001; Cucinotta and Chappell, 2010; Huang et al., 2019). In the present context, we can and shall identify negative second derivatives with concavity (Fig. 1).

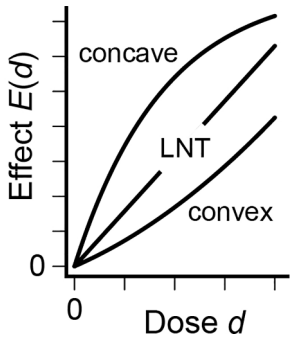

Fig. 1. Linearity and curvilinearity. The figure is schematic, mainly intended to illustrate concavity and convexity. The concave line is the one of main interest. For example, our one-ion DERs are concave. For the HZE one-ion NTE-also DERs the slope at low doses is extremely high and the concavity is so large it looks like a kink in many of our later figures. Abbreviations used here: DER – dose-effect relation; HZE – high charge and energy; LNT – linear no threshold; NTE – non-targeted effect(s).

1.4. Synergy analysis

1.4.1. Simple effect additivity (SEA) and its replacements

Given one-ion DERs, it was possible to check the two-ion mixtures for synergy. Synergy theory compares an experimentally-observed mixture DER with a neither-synergy-nor-antagonism (NSNA) baseline mixture DER calculated from the mixture's components' one-ion DERs.

Researchers in pharmacology and toxicology have known for a very long time (e.g. Fraser, 1872; Loewe and Muischnek, 1926) that the "obvious" method of analyzing mixture effects with the SEA approach to synergy – namely just adding component effects – is unreliable when some mixture components' one-agent DERs are highly curvilinear. This problem is reviewed, e.g., in Zaider and Rossi (1980), Berenbaum (1989), Foucquier and Guedj (2015), and Huang et al. (2019). Many different replacements for SEA synergy theory are now used in biology to plan and interpret mixture experiments, as reviewed, for example, in Ham et al. (2018) and Huang et al. (2019).

1.4.2. Incremental effect additivity (IEA) synergy theory

The version of IEA synergy theory used in this paper was introduced in Ham et al. (2018). Huang et al. (2019) studied how it could be applied to murine HG tumorigenesis once mixture data became available. "Incremental" refers to the fact that the first derivatives of one-ion DERs play an essential role in IEA synergy theory. The underlying idea was suggested by the Vancouver radiobiologist G. K. Lam in 1987 (Lam,

1987). A one-ion DER slope defines a linear relation between a sufficiently small dose increment and the corresponding effect increment. Thus, by analyzing sufficiently small increments, one can circumvent the curvilinearities that plague SEA synergy theory.

A systematic analysis of slopes requires using ordinary differential equations (ODEs). Implementing Lam's insight has become practical because computers have become very adept at integrating non-linear ODEs. However, Lam did not use ODEs in his proposed replacement for SEA (Lam, 1994).

1.4.3. Overview of relevant synergy theory methods

The paper's synergy analysis is previewed in Fig. 2.

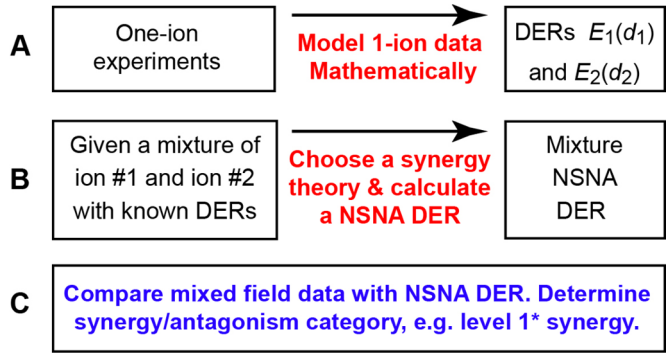

Fig. 2. Synergy analysis for two-component GCR-simulating mixed beams. The figure summarizes the approach used in this paper and would apply much more generally throughout biology if "ion" were replaced by "agent" every time "ion" appears in the figure. Recall that NSNA is the abbreviation for "neither synergy nor antagonism". WebSup1 subsection W2.5 explains the terminology in box C.

Importantly, Fig. 2 applies to DERs, which by definition have the background tumor prevalence in unirradiated mice subtracted out. We reasoned that synergy, if it occurs systematically, probably involves synergy based on ion track structure properties, not on properties of the unknown agents that cause background prevalence.

1.4.4. Choosing IEA synergy theory

The paper's HZE NTE-also one-ion DERs are highly curvilinear. Therefore, in view of the issues reviewed in subsection W1.4.1, we had to choose a replacement for SEA synergy theory; we had a choice of many inequivalent replacements. IEA synergy theory was chosen. WebSup1 subsection W1.4 covers some of the extensive literature on different synergy theories; it indicates features that most synergy theories have in common as well as ways in which they differ; it explains criteria, general or specific to radiobiology, for choosing among different synergy theories; it states our motivations for choosing IEA synergy theory; and it lists pros and cons of that choice, some of which are also discussed in later parts of this paper itself.

2. Materials and methods

2.1. Customized software

We use the open source programming language R (Matloff, 2011). Initially designed for statistical calculations, R has now gained wide acceptance among modelers (IEEE, 2014). Our customized programs can be freely downloaded, without needing to register, from the public GitHub repository https://github.com/rainersachs/LSSR_HG_2019. The reader can then use and modify them under the GNU GPL v3.0 license, which is widely respected for facilitating software sharing with a minimum of strings attached. Detailed instructions for using the scripts are in WebSup1 subsection W2.1.

Readers can thus freely access the data we used, check our calculations, and evaluate our conclusions critically. We suggest the following points: (a) cooperation among different mathematical and computational modeling groups is essential to reach an evidence-based consensus that deserves high credibility within the radiobiology community; (b) nowadays the only way to reach such a consensus is proactive transparency in the form of open source, freely available, freely modifiable customized software; and (c), nowadays such software often carries more information than any other kind of presentation – words, figures, animations, even equations.

2.2. The BEVALAC-NSRL HG data set

The approach in Section 2.1 to acquire the data used is recommended, because it enables data access in context, where the reader can track how the data is being used in calculations. This subsection gives less informative but more immediately readable excerpts.

2.2.1. Summary of experimental design and relevant physics parameters

Table 2 enlarges Table 1 to include all one-ion nonzero-dose experiments used in the entire BEVALAC-NSRL HG data set.

Table 2
Isotopes used.

Ion	*Z*	*SKE*	*L*	*β*	Accelerator	Number[a]
		MeV/u	keV/μm			**Total = 52**
^{1}H	1	250	0.4	0.614	NSRL	5
^{4}He	2	228	1.6	0.595	Bevalac	8
^{16}O	8	350	20	0.692	NSRL	3
^{20}Ne	10	670	25	0.813	Bevalac	5
^{28}Si	14	260	70	0.623	NSRL	5
^{48}Ti	22	1000	100	0.876	NSRL	5
^{56}Fe	26	600	193	0.793	Both[b]	10
^{56}Fe	26	350	250	0.654	Bevalac	4
^{93}Nb	41	600	464	0.793	Bevalac	4
^{139}La	57	593	953	0.791	Bevalac	3

[a] Total number of one-ion experiments using this ion.
[b] Data in this row comes from both the Bevalac and NSRL. Details on the method used to combine the Bevalac and the NSRL data are given in Chang et al. (2016).

In Table 2: approximate LETs for the Bevalac rows are at the tissue depth of the HG; LETs for the NSRL rows are at the surface of the animals, which were allowed to move during irradiation in the NSRL experiments; for the "Both" row the value 193 keV/μm was assigned to the combined data (Chang et al., 2016). There are two swift light ions (SLI), namely ^{1}H and ^{4}He ions, and there are eight HZE ions. Zero-dose (i.e. control) experiments are not included in Table 2.

In addition to being used in the indicated number of one-ion experiments, ^{1}H, ^{28}Si, and ^{56}Fe were each used in two of the three mixed field experiments.

Table 3 gives the doses and dose rates used in the mixture experiments.

Table 3
Mixture dose parameters.

Ion	Z	Dose rate (cGy/min)	Dose (cGy) per experiment		
			p + Fe	Si + Fe	p + Si
^{1}H	1	20	40	–	60
^{28}Si	14	10	–	20	–
^{56}Fe	26	10	30	20	40
Total mixture dose (cGy)			70	40	100

In each of the three experiments the lighter ion was delivered first and the heavier ion last. Here p + Fe is an abbreviation, used throughout the rest of this paper, for ^{1}H + Fe. Similarly, p + Si will henceforth be used, not ^{1}H + Si. As an example of the henceforth typical terminology: in the p + Fe experiment, 4/7 of the total mixture dose is contributed by protons whose *SKE* is, as using Table 2 shows, 250 MeV/u; and 3/7 of the total dose is contributed by almost fully ionized ^{56}Fe atoms whose *SKE* is 600 MeV/u.

Readers who want the doses or animal numbers used in each of the experiments of Tables 2 and 3 but do not need the full information resulting from running our customized R suite can get the information as follows. Go to the GitHub repository referenced in Section 2.1 above. Access the file oneIon.csv, and the file mixIon.csv. Each file can be read as a spreadsheet.

2.2.2. Animal care and beam delivery procedures during the NSRL experiments in February 2018

The animal handling and irradiation procedures used in earlier acute-exposure, one-ion HG tumorigenesis experiments at NSRL are detailed in Chang et al. (2016) and La Tessa et al. (2016). Essentially the same procedures were used for later one-ion experiments in the BEVALAC-NSRL data set. The corresponding procedures for the mixed beam experiments were somewhat modified, and are described next.

In a preliminary test of the NSRL's GCR simulation capability, and prior to any experiment in which mice were exposed, three beam-fine-tuning experiments were performed. These helped smooth the way for later NSRL mixtures. Pairs of three different ion beams were delivered in rapid sequence. Initially, each of the three ion beams (250 MeV/u protons, 260 MeV/u silicon, and 600 MeV/u iron) were tuned separately to a flat dose 20 cm × 20 cm field with ± 1–3% uniformity. The proton beam was produced in the Tandem accelerator, and the silicon and iron ion beams came from the electron beam ion source. Along with careful beam tuning, parameters for a “sweet spot” were established such that the same calibration settings could be used for all three beams to facilitate returning rapidly to each beam. The main control room recorded the optimal settings we achieved for each beam. WebSup1 subsection W2.2.2 adds some details.

Female CB6F1 mice (10–12 weeks old) were exposed to ion pairs. First, the exposure was that shown in the p + Si column of Table 3; the Si + Fe column exposure followed; and finally the exposure in the p + Fe column. In each case the timing was as follows: the interval between the first (lighter) ion and the second ion was less than two minutes; each component dose lasted less than five minutes. Each HZE ion exposure was at a dose rate of ~10 cGy/min; and the proton exposures were at a dose rate of ~20 cGy/min.

Eight unanesthetized animals were loaded into plexiglass boxes perforated with holes for aeration for each radiation exposure. In addition, we exposed some animals to Si alone during this same prolonged series of exposures.

2.2.3. Differences between the NSRL exposures and GCR exposures

There is a substantial discrepancy between the HZE (i.e. Si and Fe) doses in Table 3 above and smaller HZE doses, accumulated by a space voyager from all of the HZE exposures during the entire time of a voyage to Mars (WebSup1 subsection W2.2.3). The discrepancy in HZE dose rates is also very large (WebSup1 subsection W2.2.3). The dose-rate discrepancy was unavoidable because, as indicated in Fig. 2, synergy analyses of mixed field results require one-ion DERs based on previous experiments and almost all the one-ion BEVALAC-NSRL HG data is from acute-exposure experiments at dose rates much higher than those which occur in interplanetary space (solar particle events apart).

2.3. Modeling

2.3.1. One-ion DERs

As emphasized in Fig. 2, synergy theory involves both one-ion DERs and NSNA mixture baseline DERs. Modeling the BEVALAC-NSRL HG data starts by devising and calibrating one-ion DERs. Some of our one-ion DERs have LET L as an auxiliary predictor variable, and are denoted by $E(d;L)$, or, if context insures no ambiguity, by $E(d)$.

We will describe the reasons for the approach we used to devise and calibrate our one-ion DERs in Section 2.3.5 below. WebSup1 subsection W2.3.1 comments at some length on intuitive interpretations of the one-ion DER's adjustable parameters and on previous DERs in the literature modeling earlier versions of the BEVALAC-NSRL HG data.

2.3.2. One-ion DERs: the hazard function approach

The starting point for the paper's models is a useful hazard function equation (reviewed in Cucinotta and Cacao, 2017):

$$E(d) = 1 - \exp[-H(d)]. \quad (1)$$

Here $E(d)$ is a one-ion DER and $H(d)$ is a non-negative function, which can be chosen by biophysical modeling, that defines $E(d)$ via Eq. (1). Short calculations show that if $H(d)$ obeys all the restrictions placed on DERs in Sections 1.2 and 1.3 above then $E(d)$ in Eq. (1) automatically also obeys the restrictions, i.e. can be used as a DER. For example, if $H(d)$ has slope $H' > 0$ then Eq. (1) implies $E' = H'exp[-H(d)] > 0$.

The most complicated of the one-ion DERs in this paper is an NTE-also model for HZE ions. It is defined by a $H(d;L)$ function in Eq. (1) that has three adjustable parameters and will be denoted by $H_3(d;L)$. $H_3(d;L)$ is taken to have additive NTE and TE contributions, denoted by N and T respectively, as follows:

$$H_3(d;L) = N(d) + T(d;L). \quad (2)$$

The NTE contribution, N, is taken as

$$N(d) = \eta[1 - \exp(-d/d_0)]. \quad (3)$$

Here η is an adjustable parameter and $d_0 = 5 \times 10^{-6}$ Gy. Numerical explorations show that the final results of the present paper are insensitive to d_0 as long as $d_0 \ll 0.001$ Gy. Some of the history of Eq. (3) is reviewed in WebSup1 subsection W2.3.2.

For the other additive term, $T(d;L)$, in Eq. (2) for $H_3(d;L)$ we devised a new form (Huang et al., 2019) which allowed us to reduce the number of adjustable parameters from four to three.

Specifically, we take $T(d;L)$ as LNT in dose (as an aside, note from Eq. (1) that having this LNT term in $H(d)$ does not imply a correspondently simple behavior in the actual DER). The dose is multiplied by an LET-dependent term $F(L) = a_{13}L\exp(-a_{23}L)$ involving two adjustable parameters, a_{13} and a_{23}, and having a form that has long been used when discussing LET dependence of relative biological effectiveness (RBE) for various endpoints (reviewed, e.g. in Huang et al., 2019). Thus,

$$T(d;L) = F(L)d, \text{ where } F(L) = a_{13}L\exp(-a_{23}L). \quad (4)$$

Combining Eqs. (1)–(4) gives the equation for this DER:

$$E_3(d;L) = 1 - \exp[-H_3(d;L)], \text{ where } H_3(d;L) = a_{13}L\exp(-a_{23}L)d + \eta[1 - \exp(-d/d_0)]. \quad (5)$$

There are 3 adjustable parameters, namely a_{13}, a_{23}, and η.

The second DER is an HZE TE-only DER that competes with E_3, obtained by setting the NTE parameter η in Eq. (5) equal to zero, i.e.

$$E_2(d; L) = 1 - \exp[-H_2(d; L)], \text{ where } H_2(d; L) = a_{12} L \exp(-a_{22} L) d. \quad (6)$$

The adjustable parameters are a_{12} and a_{22}. The third DER is for the low-LET SLI:

$$E_1(d) = 1 - \exp[-H_1(d)], \text{ where } H_1(d) = a_{11} d. \quad (7)$$

2.3.3. Estimating background prevalence

Henceforth background prevalence in unirradiated mice is denoted by Y_0. In principle background prevalence is usually regarded as a random variable but, for reasons specified at great length in WebSup1 subsection W2.3.3, Y_0 will here be defined as just a real number. To calculate Y_0, we use two integers, *denom* and *num*.

We define *denom* as the total number of mice at risk summed over all zero-dose experiments used as controls for the NSRL rows of Table 2 plus all zero-dose controls used for the three two-ion mixture experiments in the BEVALAC-NSRL data set. Readers who want more details on these control experiments but do not need the full information resulting from running our customized R suite, can get the information as follows. Go to the GitHub repository referenced in Section 2.1 above. Access the file controls.csv, which can, e.g., be read as a spreadsheet.

We define *num* as the corresponding total of mice that have at least one tumor at harvest time and define $Y_0 = num/denom$. The result is $Y_0 = 0.046404 \sim 4.64\%$. Treating this as a fixed scalar instead of a random variable means that we had to find a different way to account for uncertainties in Y_0. The approach used included recalculating all our results assuming $Y_0 = 2.5\%$ instead of $Y_0 = 0.046404 \sim 4.64\%$. The upshot was that none of our conclusions about synergy were substantially altered by this change. A conclusion about NTE versus TE was, however, altered in favor of NTE. WebSup1 subsection W2.3.3, gives the motivation for this kind of robustness check and very detailed information on the numerical values of the changes that did occur when using $Y_0 = 2.5\%$ instead of $Y_0 = 0.046404 \sim 4.64\%$.

2.3.4. Calibrating DER adjustable parameters

Given Y_0, the adjustable parameters in the three DERs of Section 2.3.2 were calibrated by inverse-variance-weighted non-linear least squares regression on the nonzero-dose data with Y_0 subtracted out. For the two competing HZE DERs a global fit was made using all data in all eight HZE rows of Table 2. For the SLI DER, all data in both SLI rows of Table 2 were used. The variances were calculated by Ainsworth's formula where variance $= p(1-p)/denom$ (Fry et al., 1985), and *denom* is the number of animals at risk and p is the prevalence, i.e. $p = num/denom$ with *num* being the number of at risk mice that had at least one tumor. Note that SLI data was not used in calibrating HZE DERs, nor HZE data in calibrating SLI DERs.

After an LET-dependent DER is calibrated by regression the calibrated DER can interpolate within the Z and LET values that appear in Table 2. For example, ^{48}Ti at $SKE = 1000$ MeV/u appears in Table 2, while ^{48}Ti at $SKE = 600$ MeV/u, which has an LET of about 125 keV/μm does not appear. Since the physical parameters (Z, baryon number, *SKE*, and *L*) for ^{48}Ti at $SKE = 600$ MeV/u all fall within the respective ranges that Table 2 does cover, it is assumed that, after calibration, $E_3(d; L)$ with $L = 125$ is an appropriate DER to use if one wants to extend the above NTE-also modeling to ^{48}Ti at $SKE = 600$ MeV/u when planning future experiments.

2.3.5. Considerations emphasized when devising one-ion DERs

Our primary concern when choosing the specific one-ion DERs in Section 2.3.2 above (DERs E_1, E_2, and E_3) rather than some other functional forms was to facilitate synergy analyses. Biophysical reasoning was relegated to second place.

Parsimonious models (i.e. those that have as few adjustable parameters as possible, in the spirit of Occam's razor) are often preferred in radiobiology and parsimony was our main criterion. There can be little doubt that emphasis of biophysical explanations of the data instead of parsimony, track structure analyses using a stochastic spatial process model, and nanometer-scale calculations is indispensable. The use of LET as an auxiliary predictor variable in E_2 and E_3 goes in that direction. But not very far. WebSup1 subsection W2.3.5 adds further comments on prioritizing parsimony and on the methods that were used in deciding on one-ion DERs.

A classic pharmacometrics paper (Berenbaum, 1989) has persuasively argued that synergy theory is by its nature a temporary expedient whose main purpose is to help make itself obsolete. Once one understands how and why the components of a mixture interact with each other, synergy theory for that mixture becomes needless and useless. Our choice of one-ion DERs was substantially influenced by Barenbaum's arguments. We reasoned that emphasizing parsimony is reasonable if mathematical convenience is an effective first step toward eventual biophysical understanding.

In all DER candidates considered when devising DERs the presence of one and only one adjustable parameter value less than zero led to a negative contribution to the prevalence, but each term in the DER was interpreted as describing either NTE action that increases prevalence or TE action that increases prevalence. This discrepancy led us to reject all candidate DERs that upon calibration contained a parameter with p-value > 0.05.

2.3.6. Comparing NTE-also and TE-only DERs

The competing HZE DERs (E_2 and E_3) were compared, balancing parsimony with goodness of fit, via three metrics: Akaike information coefficients (AIC) (Akaike, 1974), Bayesian information coefficients (BIC), and cross validation (Arlo and Celisse, 2010). WebSup1 subsection W2.3.6 gives details on the cross-validation calculations used.

2.3.7. Uncertainties in one-ion effects

Monte Carlo simulations (Binder, 1995) were used to calculate 95% confidence intervals (CI) for the DERs. Because it is known that neglecting correlations between calibrated parameters tends to overestimate how large CI are (Hanin, 2002; Ham et al., 2018) such correlations were taken into account by sampling from variance–covariance matrices.

After being calibrated by regression, the Eq. (7) DER $E_1(d) = 1 - \exp(-a_{11}d)$ can be interpreted as a family of curves with each curve in the family assigned a probability density. During regression a probability density function, which we denote by f, is assigned to the random variable a_{11} and for any real number a one can assign $f(a)$ to the function $1 - \exp(-ad)$, ending up with a smooth function of dose paired with an attribute $f(a)$. One can then graph the curve $1 - \exp(-ad)$ for any a (or, for that matter, perform other manipulations such as differentiation, holding a fixed). Unless explicitly stated to the contrary the function is always the one obtained by setting the adjustable parameter a_{11} equal to the mean of the random variable a_{11}. Similar comments apply to both of the competing HZE DERs, E_2 and E_3. For example, after calibration, E_2 has, instead of just one random variable a_{11}, a correlated pair (a_{12}, a_{22}). But Monte Carlo sampling from variance–covariance matrices allows one to implement the family of curves interpretation in essentially the same way as one implements it in the one adjustable parameter case.

2.4. Synergy theory calculations

Section 1.2 described the three mixture experiments whose synergy analyses are the focal point of this paper; Section 2.2 described the data set analyzed; and Section 2.3 characterized the calibrated one-ion DERs needed to initiate synergy analyses (row A of Fig. 2) The present subsection, 2.4, describes synergy analysis (rows B and C of Fig. 2).

The fact, mentioned earlier, that mice were free to move during the NSRL experiments is a confounding factor for synergy calculations. Shielding of the HG by other parts of the mouse turns a beam that is

one-ion monoenergetic at the mouse surface into a mixture at the HG (Norbury et al., 2016). In the IEA synergy theory calculations of this paper, this confounding is mitigated because, as Dae Woong Ham has proved (Ham et al., 2018), IEA synergy theory obeys the "mixmix principle", which is explained in WebSup1 subsection W1.2.f. SEA synergy theory and most of its replacements other than IEA synergy theory do not obey the mixmix principle.

2.4.1. SEA synergy calculations

This subsection describes SEA synergy theory calculations for the p + Fe mixed beam experiment. The first step in a synergy calculation is to decide on DERs for the mixture components (row A of Fig. 2 above). Protons are SLI so their DER is given by E_1, Eq. (7). In this subsection, assume the DER for Fe is E_3, Eq. (5), the NTE-also DER. A SEA NSNA prevalence, denoted by $S(d)$, where d is the total mixture dose due to both ions, is given by simply adding proton and Fe effects using the DERs:

$$S(d) = E_1(d_p) + E_3(d_{Fe}; L_{Fe}). \tag{8}$$

Here the numerics of Section 2.2.1 apply, namely: $d_p = (4/7)d$, $d_{Fe} = (3/7)d$, $0 \le d \le 70$ cGy and $L_{Fe} = 193$ keV/μm. E_1 is that member of the corresponding function family (described in Section 2.3.7) for which the adjusted parameter a_{11} is the mean value of the random variable a_{11}. The next few subsections describe the calculation of an IEA counterpart, $I(d)$, to $S(d)$.

2.4.2. Inverse functions

IEA synergy theory uses inverse functions. We denote the inverse function of a DER $E(d)$ by E^{-1}, i.e. $E^{-1}[E(d)] = d$. For example, the proton DER E is, as Eq. (7) shows, $E = 1 - \exp(-a_{11}d)$. The inverse function E^{-1} to the proton DER is obtained by the following calculation, where E represents any effect in the interval [0, 1):

$$\begin{aligned} E = 1 - \exp(-a_{11}d) &\Rightarrow \ln[\exp(-a_{11}d)] = \ln(1-E) \\ &\Rightarrow d = -\ln(1-E)/a_{11}. \end{aligned} \tag{9}$$

Thus, the inverse function expresses dose as a function of effect, a technique familiar in radiobiology, though in a quite different setting, from RBE calculations. Each DER in this paper has an inverse function since the positive-slope condition in Section 1.3 implies monotonic increase. In most cases, for example in the case of the Fe DER E_3 in the p + Fe mixture, the inverse function cannot be expressed in explicit form – Eq. (9) is unusually simple in that respect. However, computers can readily get high-quality numerical versions of E^{-1} by using sophisticated root finders, e.g. uniroot in the case of the computer language R, whose job is made easier by the fact that E^{-1} is monotonic increasing. The restrictions in Sections 1.2 and 1.3 on DERs imply $E^{-1}(0) = 0$, $E^{-1}(x) > 0$ for every real number x that obeys $0 < x < 1$, and the limit of $E^{-1}(x)$ as x approaches 1 is ∞.

2.4.3. The IEA NSNA baseline equation and DER

These preliminaries enable us to write out, for two-component mixtures, the key IEA equation which defines the IEA NSNA baseline mixture DER. Denote by $I(d)$ the total effect at total mixture dose d. The IEA equation, motivated in WebSup1 subsection W1.2, is that

$$(a)\ \ I'(d) = r_A E'_A[E_A^{-1}(I)] + r_B E'_B[E_B^{-1}(I)];\ \ (b)\ I = 0 \Leftrightarrow d = 0. \tag{10}$$

Here the sum on the right-hand side of Eq. (10a) specifies the small increment in effect I when a small increment in total mixture dose d is applied; A and B refer to the two components; r_A and $r_B = 1 - r_A$ are the respective fractions that the two components of the p + Fe mixture contribute to the total dose, namely 40/70 ~ 0.57 and 30/70 ~ 0.43 respectively; and $I(d)$ is defined by using a first order ODE rather than an analytic expression.

IEA synergy theory treats all components of a mixture on an equal footing. Note that in the term $r_A E'_A[E_A^{-1}(I)]$ the inverse function E_A^{-1} is evaluated at effect I that both mixture components acting jointly have already contributed before the incoming increment of dose arrived, rather than being evaluated at the seemingly more pertinent value, E_A, that ion A alone has already contributed. This use of I is the central assumption of IEA synergy theory. Intuitively speaking: (a) a biological system can know about the total damage I it has already sustained, but can only know about past doses d_A and d_B via I, because previous increments in d_A and d_B came in and left at almost the speed of light; (b) $E_A^{-1}(I)$ is the dose needed for ion A to do damage I all by itself, without any help from ion B; (c), $E_A^{-1}(I)$ gives ion A information about what damage ion B has already done; and (d), IEA can be defined heuristically as that synergy theory which tells an incoming increment of ion A dose the following – "if there is no special interaction between ion A and ion B, please use the recipe of Eq. (10A) to decide how much incremental damage you yourself should do if you want to take into account that ion B is also acting on our target".

WebSup1 subsection W1.2: (a) generalizes Eq. (10) to mixtures of more than two components; (b) adds motivations and intuitive interpretations of the resulting IEA equation; (c) outlines the proof that, for concave one-ion component DERs that obey the conditions in Sections 1.2 and 1.3, the IEA equation – and thus its two-component mixture special case Eq. (10) – always have only one solution $I(d)$, and this solution is well defined and well behaved for all non-negative doses; and (d), discusses a number of related issues.

2.5. Uncertainties in mixture effects

We used Monte Carlo simulations to calculate 95% CI for NSNA DERs. Conceptually the approach was very similar to the one described in Section 2.3.7 for one-ion DERs. However, the computational implementation was more difficult. The open source customized scripts available on GitHub give details on the implementation. Readers who change parameters relevant to Monte Carlo calculations in the scripts may encounter non-trivial bugs if the changes are too drastic.

Once 95% CI for NSNA DERs have been calculated they can be used to help introduce synergy categories that distinguish more clear-cut from less clear-cut synergy. WebSup1 subsection W2.5 gives the specifics.

3. Results and discussion

3.1. Preliminary comments

Figs. 3–7 below are used to summarize our main results. The curves in Figs. 3–7 all show DERs, i.e. have background effects Y_0 subtracted out. Using DERs when presenting plots emphasizes the opinion that synergy between background-prevalence-producing agents and radiation tracks is unlikely (Section 1.4.3 above). For consistency all data points shown on Figs. 3–7, together with their error bars, had to be shifted downward by amount Y_0. One-ion curves in any figure are always those characterized in Section 2.3.7. Error bars on all data points in any figure are ± 1 SD, located symmetrically around the data point due to the paper's use of Gaussian approximation (discussed in WebSup1 subsection W2.3.7b).

The prevalences and experimental ± 1 SD for the three mixture experiments are given numerically in the respective paragraphs above Figs. 5–7. Figs. 5–7 themselves repeat the same information visually and supply additional figure elements to characterize synergy theory results. The figures are supplemented by numerical results in Tables 4–6.

3.2. One-ion DERs

3.2.1. Calibrated SLI DER

The DER for SLI, Eq. (7), contains one adjustable parameter, a_{11}. Calibrating a_{11} by regression gave $a_{11} = 0.001381 \pm 0.000218$ ($p < 10^{-6}$). Fig. 3(A) shows the DER when $a_{11} = 0.001381$, and shows the data points for protons and ^{4}He ions. Fig. 3(B) indicates that for this data, dose is a more suitable predictor than fluence.

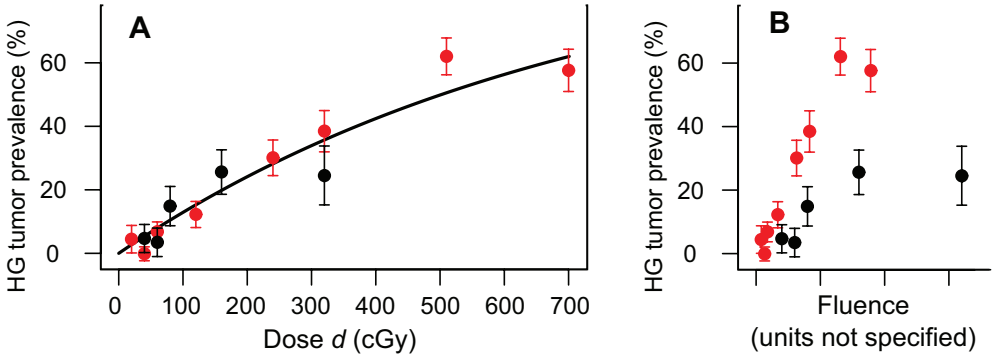

Fig. 3. SLI data and model. In this paper all one-ion beams for $Z \leq 2$ are modeled by the same one-ion DER, shown as the curve in panel A. Also shown are all the data points with their empirical error bars of ± 1 SD. Black symbols represent proton data, and red symbols represent ^{4}He ion data. The largest total dose used for these low-LET radiations is more than four times the maximum total dose of 160 cGy used for any HZE one-ion experiment in the entire BEVALAC-NSRL data set. Shifting the curve and data points upward by $Y_0 = 0.046404$ would give a figure showing total effects, rather than radiogenic effects only (see Section 3.1). Panel B shows the same data plotted as a function of fluence. (This figure should be viewed in color. Refer to the online version of this article for color figures.)

Since the ^{4}He LET is four times as big as the proton LET and fluence is proportional to d/L one can visualize panel B as having been obtained from panel A by shifting all ^{4}He points in Fig. 3 horizontally to the left until their abscissa is reduced to 0.25 times its previous value. Considering that only one adjustable parameter is used in defining E_1, Fig. 3(A) suggests that, for the SLI in the BEVALAC-NSRL HG data set, considering dose as the basic independent variable is appropriate. Fig. 3(B) suggests that fluence is here less appropriate.

3.2.2. High LET results

Calibration results for the adjustable parameters of our HZE DERs are shown in Table 4.

Table 4
Regression results for the one-ion NTE-also and TE-only HZE DERs (E_3 and E_2 respectively).

Model	Parameter	Estimate	SE	p-value	Level
E_3	a_{13} (μ keV^{-1} cGy^{-1})	8.000e−5	1.42e−5	2.81e−6	$p \ll$ e−3
	a_{23} (μ keV^{-1})	3.387e−3	6.43e−4	8.35e−6	$p \ll$ e−3
	η (%)	3.247e−2	1.04e−2	3.85e−3	$p <$ e−2
E_2	a_{12} (μ keV^{-1} cGy^{-1})	1.091e−4	1.50e−5	2.03e−8	$p \ll$ e−3
	a_{22} (μ keV^{-1})	3.941e−3	5.98e−4	1.50e−7	$p \ll$ e−3

Here "e" refers to powers of 10, e.g. 3.387e−3 = 0.00387. In statistics notation, p is the probability that the random variable representing an adjustable DER parameter after calibration is less than zero – context distinguishes it from prevalence, which in this paper is also denoted by p.

It is seen in the last two columns of Table 4 that all adjustable parameters differ significantly from 0, with $p < 0.01$. This fact should not be misinterpreted as indicating that the data set is high precision or that our DERs are clever. Instead it is mainly a consequence of the fact that when we were devising DERs, any adjustable parameter for which $p > 0.05$ was deemed grounds for rejecting the DER.

Fig. 4 shows, as an example, both calibrated HZE DERs for Fe ions with $SKE = 600$ MeV/u, so that the auxiliary predictor variable L is 193 keV/μm (Table 2). Recall from Section 3.1 that background prevalence Y_0 has here been subtracted out. Panel A uses the Estimate column of Table 4. Panel B omits the E_2 rows but adds information from the SE column. In addition to the two DERs, Fig. 4(A) also shows corresponding one-ion prevalence data.

The corresponding HZE NTE-also DER E_3 (red curve) looks as if the DER smoothness conditions given in Section 1.3 above might not hold. The slope at $d = 0$ looks like it might be infinite; in addition, it appears as if at one point there is a kink where the first derivative is discontinuous. Actually, the slope at $d = 0$ is finite though very large and there is no kink, just a small interval of very high concavity. There are

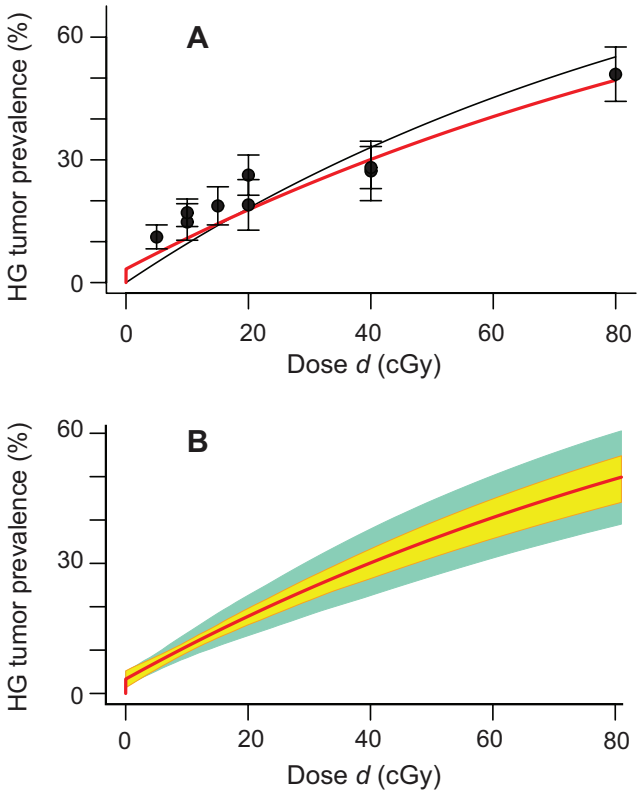

Fig. 4. HZE one-ion DER shapes and observed prevalences. Panel A shows the TE-only DER E_2 with $L = 193$ keV/μm (black curve). Experimental points for Fe at 600 MeV/u and their ± 1 SD error bars are also shown. (This figure should be viewed in color. Refer to the online version of this article for color figures.)

no points in the BEVALAC-NSRL HG data set for nonzero doses in this region, where the dose is seen to be ≪ 1 cGy. The moderately low-dose region has to be used as the only available guide as to prevalences for doses ≪ 1 cGy.

Panel B gives ribbons for the red curve in panel A. Vertical intervals on each ribbon give 95% CI for the red curve. The aquamarine broader ribbon does not take adjustable parameter correlations into account. The narrower yellow ribbon (which hides part of the aquamarine ribbon) takes adjustable parameter correlations into account.

The largest dose for Fe at 600 MeV/u used in any of the three two-ion mixture experiments was 30 cGy. Fig. 4 omits one data point (at dose 160 cGy) for the sake of better visual clarity, but that data point

Table 5
Adjustable parameter variance–covariance matrices and correlation matrices.

Model		Variance–covariance matrix			Correlations		
E_3	Parameter	a_{13}	a_{23}	η	a_{13}	a_{23}	η
	a_{13} (μm keV^{-1} cGy^{-1})	2.015e−10	7.807e−9	−8.060e−8	1	0.86	−0.54
	a_{23} (μm keV^{-1})	7.807e−9	4.138e−7	−1.862e−6	0.86	1	−0.28
	η (dimensionless)	−8.060e−8	−1.862e−6	1.091e−4	−0.54	−0.28	1
E_2	Parameter	a_{12}	a_{22}	NA	a_{12}	a_{22}	NA
	a_{12} (μm keV^{-1} cGy^{-1})	2.251e−10	7.731e−9	NA	1	0.86	NA
	a_{22} (μm keV^{-1})	7.731e−9	3.584e−7	NA	0.86	1	NA

Here "e" refers to powers of 10, e.g. 2.015e−10 = 2.015 × 10^{-10}. Of note is the correlation of −0.54 between a_{13} and η. We had expected a correlation with absolute value substantially smaller than 0.5 because the two parameters a_{13} and η refer to different dose ranges and different biophysical mechanisms.

was included in the regression calculation.

Comparing the prevalence at 80 cGy in Fig. 4(A) with the prevalence at 80 cGy in Fig. 3(A) it can be seen that the high LET Fe ions are more effective per unit dose than the low LET SLI. The ratio of prevalences at this dose is roughly 4:1. Thus the higher LET radiation is more effective at inducing murine tumorigenesis, as is of course also true for many other endpoints and pairs of radiations. The above 4:1 factor should not be confused with a quality factor. Quality factors are also obtained from comparing high LET radiations with a low LET radiation, but they do not use SLI as the low dose radiation, they consider effect rather than dose as the independent variable, and they are concerned with issues not very directly related to whether specific mixtures show synergy or not.

We were surprised to see how closely the one-ion data matched the curves in panel A of Fig. 4. We then made corresponding figures for the other seven HZE ions and found that for some of those the fit in panel A is not nearly as close. WebSup1 subsection W3.2.2 gives the Si-ion counterpart to Fig. 4 as an example.

The parameter variance–covariance and correlation matrices for the one-ion HZE DERs, are shown in Table 5.

Table 6 gives scores used to compare our one-ion HZE DERs with each other. Smaller scores are better in all cases. For example, a score of 5 is better than a score of 10 but −10 is smaller than −5 so a score of −10 is better than a score of −5.

Table 6
CV, AIC, and BIC.

Model	CV	AIC (df)	BIC (df)
E_3	0.002297	−8816 (4)	−8809.2 (4)
E_2	0.002302	−8814 (3)	−8809.3 (3)

It is seen that neither model is a clear over-all winner. Abbreviations: CV – cross validation; AIC – Akaike information criterion; df – degrees of freedom that are used up; BIC – Bayesian information criterion.

3.3. Mixture synergy analysis

The preceding subsection describes results for one-ion DERs. It thus corresponds to row A of the synergy modeling flow chart, Fig. 2. We now turn to our main results, on synergy, corresponding to rows B and C of the flow chart.

Figs. 5–7 show IEA NSNA baselines *I(d)*, and their 95% CI ribbons calculated taking adjustable parameters into account. The three figures compare *I(d)* and its yellow ribbon with observed mixture prevalence. A "star-level" terminology is introduced for categorizing how clear-cut synergy is – though concerned with a quite different issue it is somewhat similar to using p-value levels such as *** or ** for statistically significant difference from 0 at the 0.001 or 0.005 level respectively.

There will be a figure for each experiment, as follows: Fig. 5 is for the p+Fe experiment, Fig. 6 for the Si+Fe and Fig. 7 for the p+Si experiment. Each of these figures shows the prevalence, and its ± 1 SD error bar, for the mixture data point and indicates the point's synergy category as determined by its relation to the NSNA curve and NSNA 95% CI.

Fig. 5 shows results for the p+Fe mixture. The mixture prevalence (including Y_0) was 47.5% ± 7.9%. Recall from Section 3.1 that background prevalence Y_0 is subtracted out in Figs. 5–7.

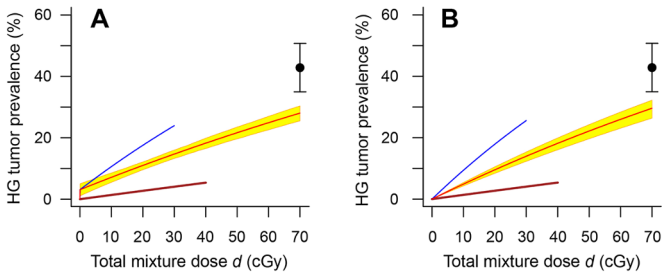

Fig. 5. The p+Fe mixture experiment shows level 1* synergy. Panel A uses the NTE-also Fe model, panel B uses the TE-only Fe model. In both panels, the following hold. The brown curve is for the proton DER and is truncated at the dose of 40 cGy that the proton beam contributed to the mixture. Similarly, the dark blue curve is for the Fe beam. The red curve is the IEA NSNA baseline and is seen to lie between the blue and brown curves. The red and blue curves start at the origin (but that is not obvious in panel A). Vertical intervals on the yellow ribbon, calculated taking adjustable parameter correlations into account, show 95% CI for the red curve, much as in the one-ion figure, Fig. 4(B). The black dot with its ± 1SD error bars is the measured prevalence in the mixture experiment after Y_0 has been subtracted out. The error bars do not intersect the yellow ribbon in either panel. (This figure should be viewed in color. Refer to the online version of this article for color figures.)

It can be seen that if the vertical length of the error bar were increased from ± 1SD to ± 1.96SD, where 1.96 is the usual Gaussian approximation to 95% CI, then an intersection with the yellow ribbon would occur. We take the facts that the bottom of the error bar is above the yellow ribbon whereas ± 1.96 SD error bars would cause an intersection as a definition of "shows 1* synergy" – the effect of the two ions combined is larger than the NSNA DER value calculated from the one-ion DERs by a "1*" margin but not by any larger margin. Thus, the NTE-also and TE-only models agree with each other that there is level 1* synergy in the p+Fe experiment.

The definition of 1* synergy in the Fig. 5 caption is generalized in WebSup1, subsection W2.5a, which gives hypothetical examples of synergy levels from 0* to 3*. For a deleterious endpoint such as tumorigenesis, increasing synergy * level means increasingly ominous news for space voyagers and space voyage planners.

Fig. 6 shows results for the Si+Fe mixture. The mixture prevalence (including Y_0) was 32.5% ± 7.41%. Unlike Figs. 5 and 7, Fig. 6 has, in panel A, one curve that is calculated using SEA, rather than IEA, synergy theory. However, this paper never uses SEA calculations apart from that one curve, and our comments here apply to IEA, rather than SEA, synergy theory unless explicitly stated to the contrary.

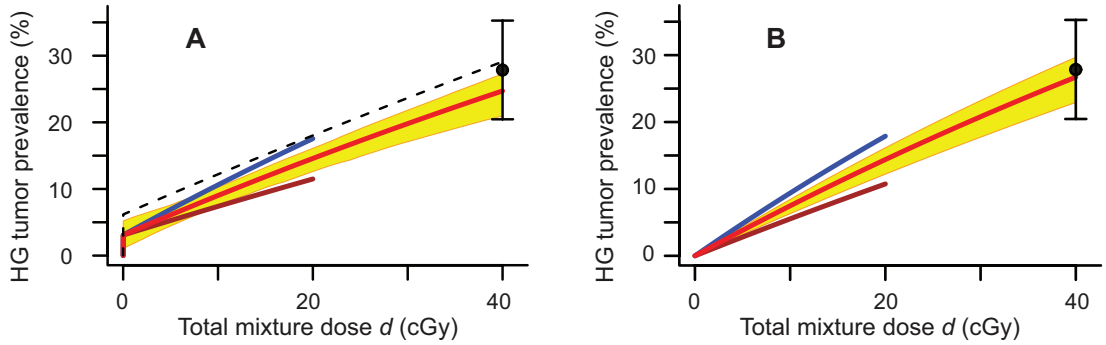

Fig. 6. The Si + Fe mixture experiment does not show significant synergy or antagonism. In both panels the blue curve is for Fe and the brown curve is for Si. The dashed black curve in panel A is the SEA (rather than IEA) mixture NSNA baseline. The black dot itself intersects the yellow ribbon, which is the definition of the category "no significant synergy or antagonism" (see WebSup1 subsection W2.5). (This figure should be viewed in color. Refer to the online version of this article for color figures.)

Importantly, it is apparent even to the naked eye that the dashed black curve in Fig. 6 lies above both the blue and the brown curves on a dose interval (A, B), where A is zero or slightly larger and B is larger than 20 cGy. In all other respects the items in the figure correspond to parallel items in Fig. 5. Thus the red curve is the IEA NSNA baseline and can be seen to lie between the blue and brown curves on almost all of the interval between 0 cGy and 20 cGy. In panel B of Fig. 6 and in Figs. 5 and 7, no SEA curve is shown because in those panels SEA and IEA curves are much closer to each other than in Fig. 6(A).

Lastly, Fig. 7 shows corresponding results for the p + Si mixture. The mixture prevalence (including Y_0) was 29.55% ± 6.88%.

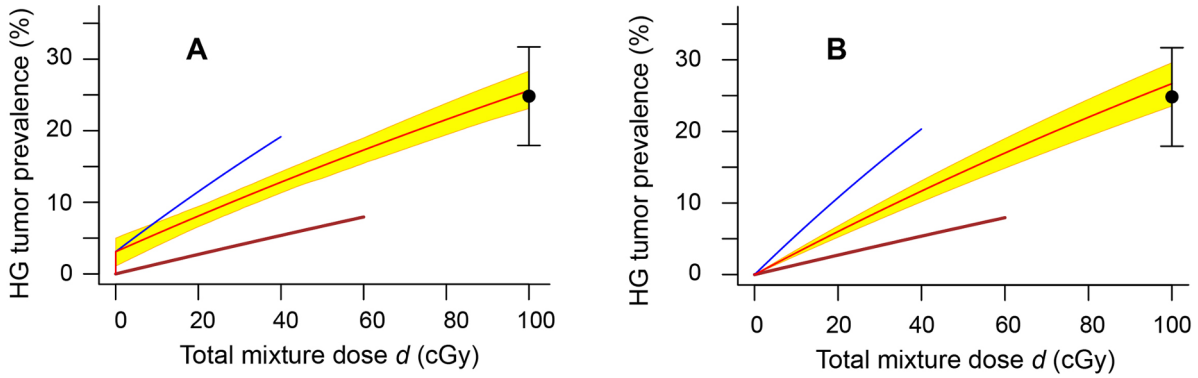

Fig. 7. The p + Si mixture experiment does not show significant synergy or antagonism. In both panels the blue curve is for Si and the brown curve is for protons. In all other respects the items in the figure correspond to parallel items in Fig. 5. (This figure should be viewed in color. Refer to the online version of this article for color figures.)

3.4. Review and discussion of the results

The main result of this paper is that one two-ion mixture experiment in the BEVALAC-NSRL HG data set showed level 1* synergy and the other two mixture experiments in the data set, both also two-ion mixture experiments, did not show significant synergy or antagonism. This subsection reviews and comments on that result and on a number of other results that emerged during the calculations.

3.4.1. Results on synergy and antagonism

For a deleterious endpoint such as tumorigenesis, synergy means additional damage. The paper and WebSup1 define various levels of synergy. Intuitively speaking, level 0* synergy is the mildest form of synergy, level 1* synergy is somewhat more ominous, level 2* is even more ominous, etc. The definition of level 1* synergy is shown in Fig. 5 as a geometric relation between observed mixture prevalence and its ± 1 SD error bars for the p + Fe mixture, compared to the calculated IEA NSNA baseline mixture curve and a yellow ribbon characterizing the 95% CI for that baseline curve. Panel A assumes that Fe action is NTE-also; panel B assumes Fe action is TE-only. The two panels agree with each other that level 1* synergy is shown. This is the only experiment that shows level 1* synergy. No synergy of level 2* or higher was shown for any experiment, whether we used our main calculations or an auxiliary calculation, described in subsection W2.3.3, that was carried out to check the robustness of our results.

In Fig. 6, which shows results for the Si + Fe mixture, both panels agree with each other that neither synergy nor antagonism is shown, when using either the main calculation or the robustness-probing auxiliary calculation. The same is true for Fig. 7, which shows results for the p + Si mixture. So our main result – one mixture experiment shows level 1* synergy and two others show neither synergy nor antagonism – holds robustly.

3.4.2. CI

When calculating 95% CI the conceptually correct procedure is to take correlations between one-ion DER adjustable parameters into account instead of neglecting them (Hanin 2002), reviewed in Ham et al. (2018).

The results shown in Fig. 4(B) of the present paper, the results shown in WebSup Fig. W3.1B, as well as other results (not shown) obtained during exploratory calculations, confirmed that the conceptually correct calculations can lead to substantially tighter CI for one-ion DERs and for mixture IEA NSNA baseline DERs. This fact has been pointed out previously (Ham et al., 2018; Huang et al., 2019) but only for mixtures that were hypothetical. It now seems that, for HZE ions with NTE-also DERs and for mixture NSNA DERs where much of the dose is contributed by such ions, tightening by a factor of about two as in Fig. 4(B) may be typical.

We suggest taking the parameter correlations into account can and should be considered the default error analysis method throughout radiobiology, whether or not IEA or any other synergy theory is being used, whether or not HZE ions are involved. The suggestion does not concern synergy or antagonism among the ions in the BEVALAC-NSRL HG data set. Instead it concerns a broader and in our opinion more important topic – the implications of using proper statistics methodology – that happens to be well illustrated by this paper's synergy theory results.

Apart from Fig. 4(B) the figures that helped lead us to the above suggestion were not shown in the paper. Readers familiar with R can obtain most of the other figures as follows. Download the customized open source suite that is in the GitHub public repository rainersachs/LSSR_HG_2019. The script plots.R generates the paper's plots, including Figs. 4(B) and 5. Reading and running the chunks of plots.R that generate Figs. 4(B) and 5(A) supplies templates that can be mimicked to get additional examples that are informative about 95% CI intervals obtained when neglecting parameter correlations.

3.4.3. Replacing SEA synergy theory with IEA synergy theory

Many of the results being reviewed here used IEA synergy theory, our preferred replacement for SEA synergy theory. The reasons for replacing SEA and the reasons for utilizing IEA have been previously published (Ham et al., 2018; Huang et al., 2019). In addition, they are reviewed at length in WebSup1, subsection W1.4. The overall picture painted in the two references and WebSup1 subsection W1.4 was left almost intact by the calculations of the present paper. There were two comparatively minor touch-ups, one pro-IEA, one anti-IEA, as follows.

In Fig. 6 panel A it was shown that the IEA NSNA mixture baseline DER lies nicely between the two one-ion DERs of the mixture's two components, while the SEA NSNA mixture baseline DER lies above both. Any assertion that no synergy is involved when a mixture produces a higher effect than either of its two components could produce if it contributed all the mixture dose by itself (with the other component not even being used) is a symptom of an unacceptable synergy theory. So Fig. 6 panel A confirms, for an actual rather than just a hypothetical mixture, that SEA needs to be replaced.

More specifically, the fact that the red (IEA) curve lies between the blue and brown curves in Fig. 6(A) agrees with the key qualitative idea that, given a mixture of two agents, synergy occurs when the agents interact in such a way as to reinforce each other's action – absent reinforcement, and absent interference, a 50–50 mixture of the agents ought to produce just about the average of their respective effects and thus lie just about half way between them. Since the dashed black (SEA) curve actually lies above both of the one-ion curves SEA synergy theory fails altogether to be a quantification of that key qualitative idea when applied to the Si + Fe mixture under the assumption that both HZE have NTE-also action.

Turning to the anti-IEA touch-up, the present paper's methods and results made clear that one IEA weakness, its need for monotonically increasing one-ion DERs, was more important than we had previously realized. In Section 1.3 of the paper we imposed monotonic increase on all our DERs via a condition that the slope of a DER always be positive. Then in devising one-ion DERs (Section 2.3.2) we had to, for consistency's sake, confine attention to candidate DERs that are monotonically increasing. Now any synergy calculation involves choosing one-particle DERs before even starting to consider mixed field results (Fig. 2). Consequently, the monotonically increasing constraint at that stage of the calculation was unmotivated, and it impeded our search for appropriate DERs. For example, some important DERs in the literature are not monotonically increasing (Cucinotta and Chappell, 2010; Cucinotta et al., 2013) but we could not use them as candidates nor even properly take into account corresponding results obtained by the use of such DERs.

Our IEA approach to synergy also has other limitations. These were summarized in Huang et al. (2019) and are reviewed in WebSup1 subsection W1.4, especially W1.4e. For example, one of the other limitations is that, since IEA relies heavily on numerical rather than analytical methods, it is difficult to get a global overview of how IEA NSNA baseline mixture DERs behave for all relevant adjustable parameter sets. Our views on these other limitations were not changed by the research reported in the present paper.

The bottom line is the following. SEA is, for many mixtures, debarred from use by fatal weaknesses. The search, described in Section 2.3.2, for one-ion DERs showed that IEA has a weakness that, while not fatal, can be quite detrimental. An attempt, described in the web supplement of Ham et al. (2018), to address this weakness of IEA synergy theory is still under consideration. It may or may not eventually be successful.

3.4.4. Parsimony

The paper emphasized parsimony of the one-ion DERs which are needed when initiating a synergy analysis (row A of Fig. 2). The quality of the fit of our three one-ion DERs was considered adequate for the synergy analysis of the three two-ion mixtures. The paper did not investigate whether alternative one-ion DERs, e.g. DERs based on the Katz amorphous structure approach (reviewed in Cucinotta and Chappell, 2010 and Cucinotta and Cacao, 2017), might have better scores in a systematic evaluation that includes balancing parsimony against the goodness of fit.

The SLI modeling was parsimonious in the sense that only one adjustable parameter was used for the DER E_1, but also in the sense that a single LET-independent DER was used for both protons and ^{4}He ions. Fig. 3 shows that this would not have been reasonable if we had used fluence as our independent variable. Fluence is an important parameter when considering the effects of ion tracks (Curtis et al., 1992), especially when stochastic process calculations to assign probabilities to small integer geometric hit numbers are called for. However, in each experiment described by Fig. 3, the total number of tracks involved is very large, averaging instead of using stochastic process calculations is therefore called for, and thus there is no reason to suppose fluence is a more appropriate predictor variable than dose. That fluence effect relations would be manifestly less appropriate than a single LET-independent DER did come as a surprise. Intuitively speaking, the DER LET-independence suggests that whatever the mechanism that makes tumors may be, the mechanism is more sensitive to the amount of energy that one hit deposits than assuming linear proportionality to uncorrelated geometric hit number would imply – i.e. suggests that a given amount of energy is more tumorigenic if concentrated in a few hits (or a few highly correlated series of hits along one track) than if it were distributed among more and smaller uncorrelated hits.

3.4.5. Multi-component mixtures

The BEVALAC-NSRL HG data set as yet contains no mixtures with more than two components so none of this paper's calculations relevant to synergy involved more components. But inevitably our analyses, e.g. those Si and Fe mixtures, raised a question: were our results merely sui generis – narrowly confined to the specific mixtures analyzed – or did they also give some useful information on other mixtures, including mixtures with more than two components, e.g. mixtures all of whose components are HZE ions? At least one part of the two-component analysis, namely the two-component IEA ODE initial value problem Eq. (10), generalizes easily, to the initial value problem for the multi-component IEA ODE, Eq. (W1.2.1) in WebSup1. In contrast, quite a few synergy theories have to date been defined only for the two-component mixture case (reviewed in Ham et al., 2018).

3.4.6. Track structure vs. phenomenological approaches to synergy theory

Unfortunately, this paper's use of track structure concepts is inadequate. In Section 2.3.5 we argued that biophysical interpretation of our synergy theory results would likely require track structure analyses using a stochastic spatial process model of track structure and

emphasizing nanometer-scale calculations, but our use of LET as an auxiliary variable went only a very slight distance in that direction. WebSup1 subsection W3.3 gives an argument that is based on a stochastic spatial process model of track structure but does not give any actual numerical calculations to back up the argument, only qualitative comments known to apply in mathematical stochastic process theory. The track-structure discussion in Section 3.4.4 is likewise missing specific quantifications. In short, this paper does not enrich synergy analysis with track structure analysis in a way that the fundamental importance of track structures in the etiology of GCR-simulating damage probably calls for.

4. Conclusions

For the foreseeable future radiobiologists studying mixed radiation field effects will almost inevitably emphasize possible synergy or antagonism among the different radiation qualities in the mixture. That has usually been the emphasis in the past. Synergy theory is needed to plan experiments and to interpret their results. Therefore trying to find a systematic quantitative approach to synergy theory general enough to cover most cases of radiobiological interest and precise enough to enable credible estimates of synergy significance is worthwhile. This paper has documented some progress in that direction in addition to implementing its primary function as an interim report on the first three mixture experiments in the BEVALAC-NSRL HG data set.

Whether mixing GCR components often leads to 1* or even more ominous synergy for tumorigenesis (or for other deleterious endpoints) is not known. We suggest that finding 1* synergy for one mixture out of three, with the other two showing neither synergy nor antagonism, is not a major red flag. Our calculations did not uncover any experimental or theoretical reasons to suppose that more ominous synergy will occur for other mixtures.

The question of whether level 2* or higher level synergy occurs probably deserves more investigation. Especially important would be synergy among HZE ions, in view of their high RBE for many endpoints.

There are ongoing and planned GCR-simulating-mixture studies, not only those of our own group studying murine HG tumorigenesis but many other groups worldwide studying many other endpoints. Often the studies do include the prerequisites for systematic synergy analyses that include synergy star-level estimates. Presumably outputs will include, for a number of different (mixture, deleterious-endpoint) pairs, determining whether or not synergy occurs and being able to assign a synergy star-level category if synergy does occur. That should help guide practical further steps for planning future missions into deep space.

Declaration of competing interest

The authors declare that they have no known competing financial interests or personal relationships that could have appeared to influence the work reported in this paper.

Acknowledgments

EAB, PYC, and RKS gratefully acknowledge funding support from NASA [Grant no. NNJ16HP22I (EAB)], under the auspices of the U.S. Department of Energy Office of Science under Contract No. DE-AC02-05CH11231. EGH, RYW, LX, GY, BZ, DWH, YL and RKS are grateful to the UC Berkeley Undergraduate Research Apprenticeship Program (URAP) for making our research classes available and successful. We thank Dr. F.A. Cucinotta, Dr. M. Hada, L. Chappell, and Dr. J.H. Mao for useful discussions, L. Chappell and Dr. F.A. Cucinotta for clarifying some details of the data sets, and Dr. J. Miller for kindly making available a table of LET and range for atomic nuclei of a given specific kinetic energy. A large group of individuals were involved in conducting this three rapidly-sequential-beam experiment. EAB, PYC and RKS would like to express our gratitude to Drs. Jian-Hua Mao, Megumi Hada, Adam Rusek, Peter Guida, Chiara La Tessa, Michael Sivertz as well as Chris Rosen, James Bakke, Amber Grover, Deborah Snyder, Kathleen Bjornstad, Andrew Beitman, and Jordan Rhone for their dedication and expert assistance. We also acknowledge the support of the Animal Care Facilities at Brookhaven National Laboratory, Lawrence Berkeley National Laboratory, and SRI International.

Supplementary materials

Supplementary material associated with this article can be found in the online version at doi:10.1016/j.lssr.2020.01.001.

References

Akaike, H., 1974. "A new look at the statistical model identification." IEEE Trans. Autom. Control 19 (6), 716–723.
Alpen, E.L., Powers-Risius, P., Curtis, S.B., DeGuzman, R., 1993. "Tumorigenic potential of high-Z, high-LET charged-particle radiations." Radiat. Res. 136 (3), 382–391.
Alpen, E.L., Powers-Risius, P., Curtis, S.B., DeGuzman, R., Fry, R.J., 1994. "Fluence-based relative biological effectiveness for charged particle carcinogenesis in mouse Harderian gland." Adv. Space Res. 14 (10), 573–581.
Arlo, S., Celisse, A., 2010. "A survey of cross-validation procedures for model selection." Stat. Surv. 4, 40–79.
Berenbaum, M.C., 1989. "What is synergy?" Pharmacol. Rev. 41 (2), 93–141.
Binder, K., 1995. Introduction: general aspects of computer simulation techniques and their applications in polymer physics. In: Binder, K. (Ed.), Monte Carlo and Molecular Dynamics Simulations in Polymer Science. Oxford University Press, Oxford.
Brenner, D.J., Little, J.B., Sachs, R.K., 2001. "The bystander effect in radiation oncogenesis: II. A quantitative model." Radiat. Res. 155 (3), 402–408.
Chang, P.Y., Cucinotta, F.A., Bjornstad, K.A., Bakke, J., Rosen, C.J., Du, N., Fairchild, D.G., Cacao, E., Blakely, E.A., 2016. "Harderian gland tumorigenesis: low-dose and let response." Radiat. Res. 185 (5), 449–460.
Cucinotta, F.A., Chappell, L.J., 2010. "Non-targeted effects and the dose response for heavy ion tumor induction." Mutat. Res. 687 (1–2), 49–53.
Cucinotta, F.A., Kim, M.H., Chappell, L.J., 2013. Space Radiation Cancer Risk Projections and Uncertainties – 2012. NASA Center for AeroSpace Information, Hanover, MD. http://ston.jsc.nasa.gov/collections/TRS.
Cucinotta, F.A., Cacao, E., 2017. "Non-Targeted effects models predict significantly higher mars mission cancer risk than targeted effects models." Sci. Rep. 7 (1), 1832.
Curtis, S.B., Townsend, L.W., Wilson, J.W., Powers-Risius, P., Alpen, E.L., Fry, R.J., 1992. "Fluence-related risk coefficients using the Harderian gland data as an example." Adv. Space Res. 12 (2–3), 407–416.
Foucquier, J., Guedj, M., 2015. "Analysis of drug combinations: current methodological landscape." Pharmacol. Res. Perspect. 3 (3), e00149.
Fraser, T.R., 1872. "Lecture on the Antagonism between the actions of active substances." Br. Med. J. 2 (618), 485–487.
Fry, R.J., Powers-Risius, P., Alpen, E.L., Ainsworth, E.J., 1985. "High-LET radiation carcinogenesis." Radiat. Res. 8, S188–S195.
Ham, D.W., Song, B., Gao, J., Yu, J., Sachs, R.K., 2018. "Synergy theory in radiobiology." Radiat. Res. 189 (3), 225–237.
Hanin, L., 2002. "Identification problem for stochastic models with application to carcinogenesis, cancer detection and radiation biology." Discrete Dyn. Nat. Soc. 7 (3), 177–189.
Hatzi, V.I., Laskaratou, D.A., Mavragani, I.V., Nikitaki, Z., Mangelis, A., Panayiotidis, M.I., Pantelias, G.E., Terzoudi, G.I., Georgakilas, A.G., 2015. "Non-targeted radiation effects in vivo: a critical glance of the future in radiobiology." Cancer Lett. 356 (1), 34–42.
IEEE. (2014). "Inst. Electric and Electronic Engineers: Top 10 Programming Languages. "Retrieved 03/2015, fromhttp://spectrum.ieee.org/computing/software/top-10-programming-languages.
Huang, E.G., Lin, Y., Ebert, M., Ham, D.W., Zhang, C.Y., Sachs, R.K., 2019. "Synergy theory for murine Harderian gland tumours after irradiation by mixtures of high-energy ionized atomic nuclei." Radiat. Environ. Biophys. 58 (2), 151–166. https://doi.org/10.1007/s00411-018-00774-x.
Kim, M.H., Rusek, A., Cucinotta, F.A., 2015. "Issues for simulation of galactic cosmic ray exposures for radiobiological research at ground-based accelerators." Front. Oncol. 5, 122.
La Tessa, C., Sivertz, M., Chiang, I.H., Lowenstein, D., Rusek, A., 2016. "Overview of the NASA space radiation laboratory." Life Sci. Space Res. 11, 18–23.
Lam, G.K., 1987. "The interaction of radiations of different LET." Phys. Med. Biol. 32 (10), 1291–1309.
Lam, G.K., 1994. "A general formulation of the concept of independent action for the combined effects of agents." Bull. Math. Biol. 56 (5), 959–980.
Loewe, S., Muischnek, H., 1926. "Ueber kombinationswirkungen. I. Mitteilung hilfsmittel der fragestellung." Archiv. Exp. Pathol. Pharm. 114, 313–326.

Matloff, N., 2011. The Art of R Programming. No Starch Press, San Francisco.
Norbury, J.W., Schimmerling, W., Slaba, T.C., Azzam, E.I., Badavi, F.F., Baiocco, G., Benton, E., Bindi, V., Blakely, E.A., Blattnig, S.R., Boothman, D.A., Borak, T.B., Britten, R.A., Curtis, S., Dingfelder, M., et al., 2016. "Galactic cosmic ray simulation at the NASA space radiation laboratory." Life Sci. Space Res. 8, 38–51.
Norbury, J.W., Slaba, T.C., Aghara, S., Badavi, F.F., Blattnig, S.R., Clowdsley, M.S., Heilbronn, L.H., Lee, K., Maung, K.M., Mertens, C.J., Miller, J., Norman, R.B., Sandridge, C.A., Singleterry, R., Sobolevsky, N., et al., 2019. "Advances in space radiation physics and transport at NASA." Life Sci. Space Res. 22, 98–124.
Slaba, T.C., Blattnig, S.R., Norbury, J.W., Rusek, A., La Tessa, C., 2016. "Reference field specification and preliminary beam selection strategy for accelerator-based GCR simulation." Life Sci. Space Res. 8, 52–67.
Zaider, M., Rossi, H.H., 1980. "The synergistic effects of different radiations." Radiat. Res. 83 (3), 732–739.